frontiers | Frontiers in Earth Science

ORIGINAL RESEARCH
published: 26 April 2022
doi: 10.3389/feart.2022.875466

End-Triassic Extinction in a Carbonate Platform From Western Tethys: A Comparison Between Extinction Trends and Geochemical Variations

Simona Todaro[1], Manuel Rigo[2,3], Pietro Di Stefano[1], Alessandro Aiuppa[1] and Massimo Chiaradia[4]*

[1]Department of Earth and Marine Sciences, University of Palermo, Palermo, Italy, [2]Department of Geosciences, University of Padova, Padova, Italy, [3]IGG—CNR, Padova, Italy, [4]Department of Earth Sciences, University of Geneva, Geneva, Switzerland

The Triassic/Jurassic boundary section cropping out at Mt Sparagio in north-western Sicily (Italy) consists of a thick and continuous peritidal succession typical of a Tethyan carbonate platform. The combined chemostratigraphic and biostratigraphic study of this section allowed us to parallel the environmental variations inferred by the isotopic records and the extinction trends recorded by the benthic organisms. In the studied section, the isotope data of C, O, and S are indicative of serious environmental perturbations related to the Central Atlantic Magmatic Province (CAMP) activity, as recorded worldwide. Two negative excursions in the C-curve (Initial-CIE and Main-CIE) confirm the acidification processes that affected the benthic community. Moreover, the oxygen isotopes curve indicates a strong warming-trend that corresponds to the reduction in biodiversity and size of the megalodontoids in the upper part of the Rhaetian beds, probably due to the deterioration of the photosymbiotic relationships of these pelecypods. We here present some novel isotope data (Zn, Pb, Sr) from the Mt Sparagio section that offer additional clues on a tight control of CAMP volcanism on the End-Triassic Extinction.

Keywords: Triassic-Jurassic boundary, end Triassic extinction, large igneous province, mass extinction, Zn-Sr-Pb isotope, Sicily

OPEN ACCESS

Edited by:
Haijun Song,
China University of Geosciences Wuhan, China

Reviewed by:
Huyue Song,
China University of Geosciences Wuhan, China
Shijun Jiang,
Hohai University, China

****Correspondence:***
Simona Todaro
simona.todaro@unipa.it

Specialty section:
This article was submitted to Sedimentology, Stratigraphy and Diagenesis, a section of the journal Frontiers in Earth Science

Received: *14 February 2022*
Accepted: *24 March 2022*
Published: *26 April 2022*

Citation:
Todaro S, Rigo M, Di Stefano P, Aiuppa A and Chiaradia M (2022) End-Triassic Extinction in a Carbonate Platform From Western Tethys: A Comparison Between Extinction Trends and Geochemical Variations. Front. Earth Sci. 10:875466. doi: 10.3389/feart.2022.875466

INTRODUCTION

The End-Triassic Extinction (ETE) is one of the Big Five mass extinction events documented during the Phanerozoic, which occurred close to the Triassic/Jurassic boundary (TJB) at about 201 Ma (Sepkoski Jr, 1994; Hesselbo et al., 2002; Blackburn et al., 2013; Lindström, 2016). Several climate and environmental perturbations occurred at the end of Triassic: a global warming estimated at 3°–4°C seems to be the result of CO_2 and CH_4 release in the atmosphere by volcanism (McElwain et al., 1999; Beerling and Berner, 2002; Todaro et al., 2018; Song et al., 2021); subaerial deposits covered the end-Triassic platform deposits implying a sea level fall (Hallam, 1997), even if its global extent is still under discussion; a decrease of ocean water circulation (Huynh and Poulsen, 2005) and widespread anoxia involved many semi-enclosed basins of Europe (Luo et al., 2018) and the mid-depth waters of oceans (Jost et al., 2017; He et al., 2020); a low oxygen conditions also in shallow water setting from western Tethys (He et al., 2022); a perturbation in the carbon cycle induced by an increase in atmospheric pCO_2 (Capriolo et al., 2021), resulted in a acidification of the ocean involved mainly bio-calcifiers organisms, such as corals, sponges and benthic bivalves, causing their extinction (Greene et al., 2012; Todaro et al., 2018). A decrease in carbonate

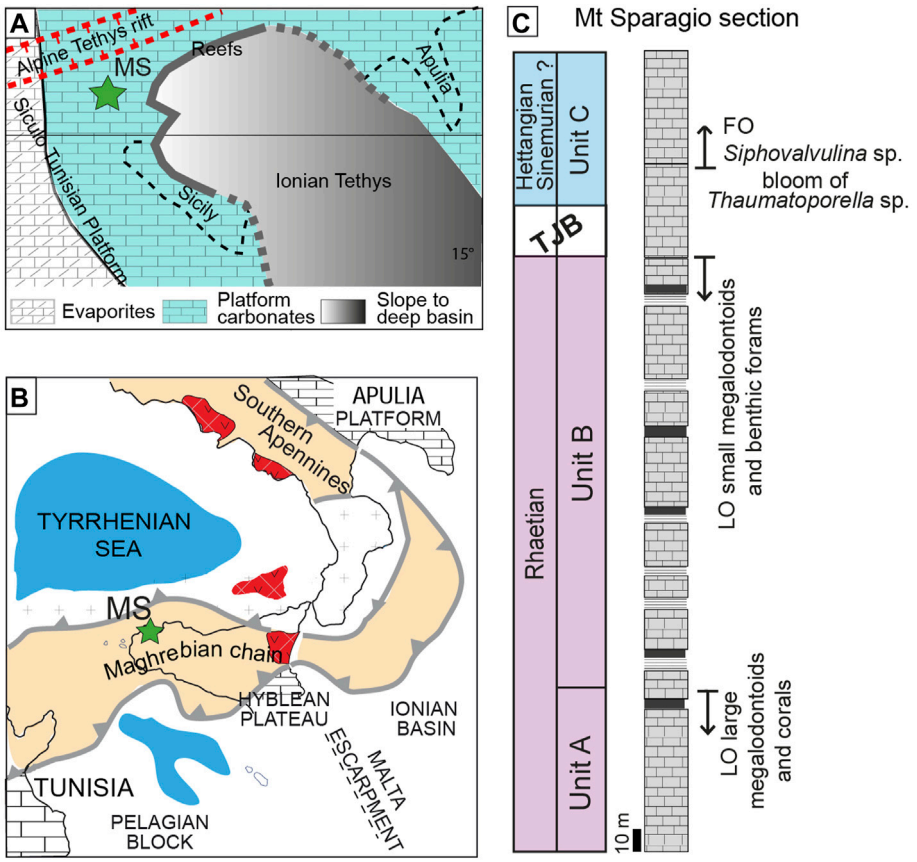

FIGURE 1 | (A) Paleogeography of the central Mediterranean area during the Late Triassic (modified after Di Stefano et al., 2015; paleolatitude after Muttoni et al., 2015). **(B)** Schematic structural map of the Central Mediterranean area. **(C)** The three informal units described in the Mt Sparagio section differentiated on the basis of the fossil associations in the subtidal facies (Modified after Todaro et al., 2018).

productivity is also observed in several stratigraphic sections from Panthalassa (Guex et al., 2004; Ciarapica, 2007; Galli et al., 2007; Wignall et al., 2007; Ruhl et al., 2009) and the Tethyan realm in which the lithologies show a decrease of wt% carbonate at TJB. All of these events might have contributed to the end Triassic mass extinction (ETE). However, the causes of the ETE are still unclear and debated, and it is largely accepted that this mass extinction is linked to the emplacement of a large igneous province known as Central Atlantic Magmatic Province (CAMP) (Marzoli et al., 1999, 2004; Wignall, 2001; Deenen et al., 2010; Schaller et al., 2011; Callegaro et al., 2014; Davies et al., 2017).

The biotic response to the environmental changes during the Late Triassic is recorded both in marine and terrestrial successions. Recent studies have demonstrated in detail two extinction pulses recorded by both marine and terrestrial realms (Wignall and Atkinson, 2020; Lindström, 2021). If on land the climatic changes led to a turnover of megaflora (McElwain et al., 1999; Lindstrom, 2021), in the marine realm high rates of extinction were recorded by benthic biocalcifiers such as bivalves, foraminifers, corals and sponges (e.g., Kiessling et al., 2007; Greene et al., 2012; Todaro et al., 2018). The main cause of the biocalcification crises was correlated to CO_2-induced acidification processes triggered by CAMP volcanism (Van De Schootbrugge et al., 2008; Todaro et al., 2018). Increasing CO_2 in the atmosphere is thought to have caused an alteration of the carbon cycle recorded by negative trends of the $\delta^{13}C$ curve (Ruhl et al., 2011; Bachan et al., 2012; Larina et al., 2021). Three major negative excursions known in literature as "Precursor" (Ruhl and Kürschner, 2011), "Initial" and "Main" CIEs (Hesselbo et al., 2002) were associated to the multiple volcanic pulses that characterized CAMP emplacement (Marzoli et al., 2004; Deenen et al., 2010; Davies et al., 2017; Zaffani et al., 2018).

This study aims to couple published data on the climatic changes, marine environmental perturbations and biotic crises recorded by a continuous Triassic-Jurassic peritidal carbonate succession from northwestern Sicily (Italy) to new isotopic data from Sr, Zn and Pb. These new results support the idea of a tight correlation between the CAMP volcanism pulses and the extinction trend at the end of Triassic.

GEOLOGICAL SETTING

The Mt Sparagio section is located in the north-western sector of Sicily (southern Italy, **Figure 1**). From the structural point of view this area, named as San Vito Peninsula, is a segment of the

Maghrebian chain and consists of a south-verging nappe pile (Giunta and Liguori, 1972; Abate et al., 1991). Each individual thrust is floored by Upper Triassic to Lower Jurassic shallow water carbonates transitional upward to pelagic carbonates of Middle Jurassic-Eocene age, with local intercalations of slope rudist limestones (Randazzo et al., 2020a; 2020b). The Upper Triassic to Lower Jurassic shallow water carbonates were part of a wide carbonate shelf that floored the south-western sector of the Tethys (i.e., Siculo-Tunisian Platform *sensu* Di Stefano et al., 2015). Part of this carbonate shelf was not involved in the Maghrebian orogeny, and today is preserved in the subsurface of the foreland areas of Sicily, e.g., the Sicily Channel and the Hyblean Plateau (Patacca et al., 1979; Antonelli et al., 1988; Todaro et al., 2021).

The internal part of the shelf was characterized by a wide subsiding peritidal area in which up to 3 km of carbonates were accumulated during Late Triassic and Early Jurassic (Patacca et al., 1979). These were transitional to evaporitic (sabkha-type) environments cropping out in the Egadi Islands, westernmost Sicily (Lo Cicero, 1986; Martini et al., 2007; Todaro et al., 2022) and are known by wells in the subsurface of the Tunisian offshore (Kamoun et al., 2001). During the Late Triassic the extensive lagoons were rimmed by a barrier reef dominated by hypercalcified coralline sponges that are recorded in several thrust sheets from Palermo to the Madonie Mountains (Senowbari Daryan et al., 2015 and references therein) (**Figure 1**). According to Zarcone et al. (2010) and Di Stefano et al. (2015) the Triassic carbonate shelf was flanked toward east by a deep and wide basin (Imerese-Sicanian Basin, *sensu* Di Stefano et al., 2015), connected to the Ionian Tethys (Finetti et al., 2005). However, due to the severe shortening induced by the Maghrebian orogeny during Neogene times, the paleogeographic relationship of this platform with the adjacent deep-water basin is subjected to different interpretations (Catalano et al., 2001).

Even if the carbonate successions pertaining to the Upper Triassic/Lower Jurassic platform are well exposed in several areas of western Sicily, a continuous section encompassing the TJB is not easy to find due to a deep erosional truncation that affected mostly the marginal sector of the rimmed platform (e.g., Palermo and Madonie Mountais, Zarcone and Di Stefano, 2010) or to local effects of dolomitization that do not allow to assess reliable bio-chronostratigraphic evaluations.

Only in boreholes from the Hyblean foreland, clear Rhaetian beds have been recognized on the base of the presence of *Triasina hantkeni* (Patacca et al., 1979). More recently the presence of Rhaetian shallow water carbonates with *Triasina hantkeni* has been reported from the Sciacca area and Mt Sparagio (Cacciatore et al., 2010). However, a careful description of the TJB section at Mt Sparagio, was first performed by Todaro et al. (2017). In this light the Mt Sparagio section can be considered as unique in Sicily.

METHODS

The descriptions of the most common macro and microfacies was based on the classification of carbonate rocks of Dunham 1969) integrated by Embry and Klovan (1972). About 200 thin sections were analysed through a Leitz Laborlux 12 Pol optical microscope under transmitted light for the petrographic and biostratigraphic characterization of the microfacies. The biostratigraphic analysis of the Mt Sparagio section was based on the biozonal schemes adopted for the Upper Triassic-Lower Jurassic sections of Tethyan inner-carbonate platform realms (Gazdzicki, 1983; De Castro, 1990; Chiocchini et al., 1994; Barattolo and Romano, 2005; Mancinelli et al., 2005; Romano et al., 2008; Coskun Tunaboylu et al., 2014).

The stable isotopic analyses were obtained from 70 samples of micritic limestone exclusively collected in the subtidal facies. O and C analyses were performed at the Department of Geosciences of the University of Padova by using GasBench II connected to the continuous flow system of a DELTA V Advantage mass spectrometer (Thermo Scientific) while S isotope analyses were performed at the Cohen Geochemistry Laboratory using an Elementar PYRO cube coupled to an IsoPrime continuous flow mass spectrometer following the procedure described by He et al. (2020) (for detailed methodology see **Supplementary Materials**).

Several laboratory analyses were carried out in order to identify any diagenetic alteration of the collected samples, including possible dolomitization. SEM (FESEM-JEOL) analyses data, performed at the Department of Chemical Engineering of University of Palermo, allowed to calculate the wt% of Mg^{2+} (0.2–0.7) confirming the absence of dolomite in the bulk samples. Cathodoluminescence observations, carried out at the School of Earth, Atmospheric and Environmental Science of Manchester University by an Olympus CCL 8200 mk3 and elemental indicators (Mn/Sr, Mg/Ca) analysed by He et al. (2022) demonstrated a minor influence of dolomitization or diagenetic processes.

These data confirm the primary nature of the collected bulk samples, supporting the use of stable isotopic analyses (O, C, S) for the Mt Sparagio section (Todaro et al., 2018; He et al., 2020; He et al., 2022).

Strontium, lead and zinc isotope analyses were carried out at the Department of Earth Sciences (University of Geneva) by Thermo Neptune PLUS Multi-Collector ICP-MS in static mode following procedures described by Chiaradia et al. (2020) for Sr and Pb and by Chiaradia et al. (2018) for Zn (see **Supplementary Materials** for detailed description).

THE MT SPARAGIO SECTION

This section is exposed along the northern slope of an east-west trending ridge about 20 km long that is part of a major thrust sheet in the southern zone of the San Vito Peninsula. This ridge is a south-dipping ramp anticline that is crosscut by NW-SE and NE-SW oriented Plio-Quaternary extensional and strike-slip faults (Nigro and Renda, 2002). However, a clear continuous sector crops out in the western part of the ridge (Mt Cocuccio, 38°3′ 44.18″ N, 12°43′9.19″ E) about 5 km north-east from the village of Custonaci. The section consists of parallel beds, the thickness of which ranges from 50 to 150 cm, dipping south from 35 to 80°. The lower part of the section is dolomitized and covered

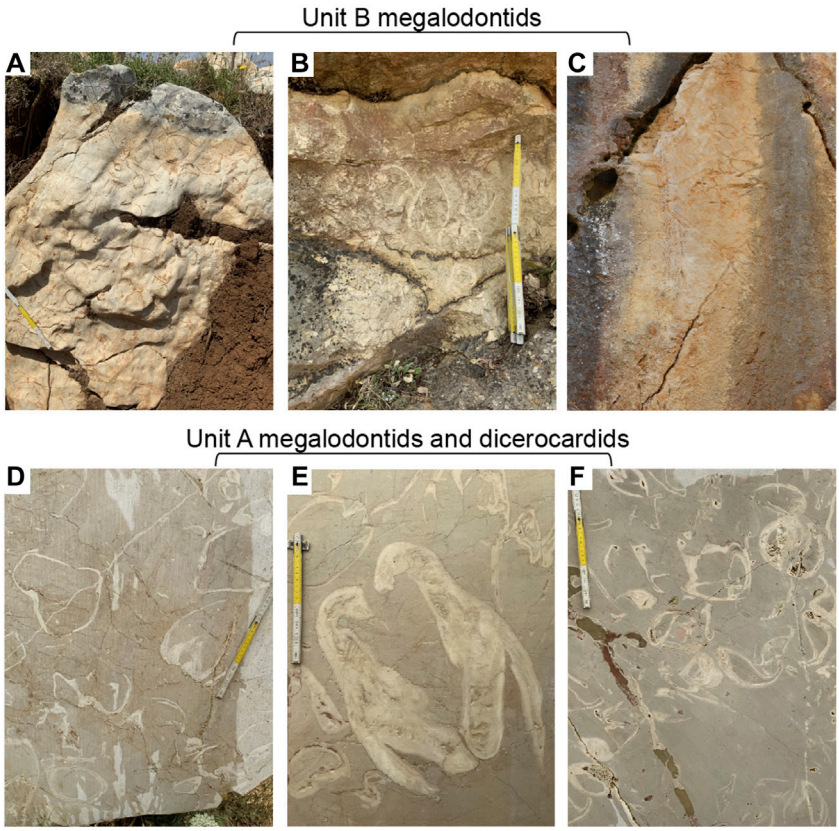

FIGURE 2 | Megalodontoids association in the Mt Sparagio section. **(A)**, **(B)** and **(C)** small megalodontids association in Unit B. **(D–F)** common presence of large megalodontids and dicerocardids shells in Unit A.

by eluvial-colluvial deposits and it is assumed to be Norian in age by the stratigraphic position. Upward, the studied section consists of 430 m thick, parallel-bedded, greyish to whitish limestones spanning the Rhaetian–Hettangian interval.

The macrofacies observations recognized peritidal carbonates formed by subtidal, intertidal and supratidal facies. Up to 13 facies-types were differentiated along the studied section (**Supplementary Table S1**). Most of the described facies are organized in shallowing-upward cycles (for a comprehensive description of facies-types and cycle stacking see Todaro et al., 2017).

On the basis of the palaeontological content in the subtidal facies, the Mt Sparagio section was divided into three informal units (**Figure 1**):

Unit A shows the common presence of large megalodontids and dicerocardids shells (**Figure 2D, E, F**), either in growth position or with disarticulated valves, in association with corals, benthic foraminifera and calcareous algae (**Figure 3A, B**). The estimated thickness of this unit is 111 m from the base of the measured section and it is well exposed along several quarries. The intertidal facies consists of stromatolite and loferite horizons that are capped by supratidal facies exhibiting black- and flat-pebble conglomerates and thick reddish-yellowish paleosoils.

Unit B shows a marked reduction in diversity and size of megalodontids whereas the dicerocardids disappear and only a few species of small megalodontids persist (**Figure 2A, B, C**). Despite this drastic biotic turnover, there are not significant variations in the benthic foraminifer assemblages and calcareous algae as observed in Unit A (**Figure 3C**). The top of Unit B is signed by an oolitic level intercalated in the subtidal facies (**Figure 3D**). Unit B reaches a thickness of 179 m. The intertidal-supratidal facies are similar to those of Unit A.

Unit C consists of shallowing-upward peritidal cycles lacking the typical fossil associations of Units A and B in the subtidal members. Only an oligotypic assemblage of encrusting algae characterizes the fossils content of the subtidal facies (**Figure 3F**). The stromatolitic facies are thicker than in the lower units representing two thirds of the total cycle thickness. Palaeosoils are thinner and less common and are represented by green-marly horizons. The total thickness of Unit C is 140 m. Between Unit B and Unit C a 10 m thick barren interval occurs consisting exclusively by calcitic spherules (up to 200 μm) (**Figure 3E**).

BIOSTRATIGRAPHY

The biostratigraphic record in the subtidal facies across all the studied section is very complete. Unit A and B, show the common

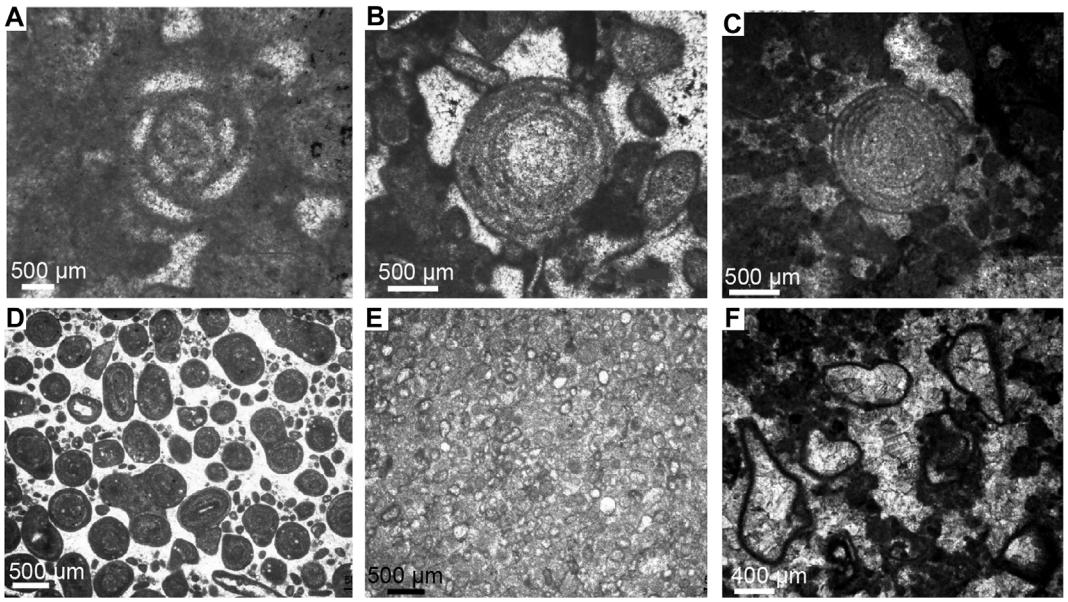

FIGURE 3 | Microfacies types in units A, B and C. **(A)** *Glomospirella* friedli in sp in Unit A; **(B)** grainstone with *Triasina hantkeni* belonging to Unit A; **(C)** grainstone with *Triasina hantkeni* of Unit B; **(D)** ooidal grainstone at the top of Unit B; **(E)** calcitic sphaerule belonging to the barren interval between Unit B and Unit C; **(F)** grainstone with *Thaumatoporella parvovesiculifera* belonging to Unit C.

presence of a benthic foraminifera association that comprises *Triasina hantkeni* (Majzon), *Auloconus permodiscoides* (Oberhauser), *Duotaxis birmanica* (Zaninetti & Bronnimann), *Tetrataxis inflata* (Kristan), *Aulotortus sinuosus* (Weynschenk), *Aulotuortus* sp., *Glomospira* sp., *Glomospirella* sp., *Trochammina* sp., *Frondicularia* sp., *Nodosaria*, sp. and *Textularia* sp. Nodular thalli of porostromata (*Cayeuxia* sp., *Orthonella* sp.) are concentrated in a few levels, whereas *Thaumatoporella parvovesiculifera* and fragments of dasycladales, such as *Griphoporella curvata*, are very rare (Todaro et al., 2017) (**Figure 3A, B, C**).

The occurrence of *Triasina hantkeni* with its large size test (up to 1 mm) allow to assign a Rhaetian age for Unit A and B (Gazdzicki, 1983; Di Bari and Rettori, 1996). The thickness of the *T. hantkeni* biozone (Unit A and B) is about 290 m, however, the base of this biozone could not be defined as the downward prosecution of the section is not exposed.

In Unit A, abundant and well preserved *Dicerocardium* spp. along with *Neomegalodon* spp. characterize the bivalve associations (**Figure 2D**). The size of the shells reaches giant dimensions up to 40 cm for dicerocardids (**Figure 2E**) and 25 cm for megalodontids (Todaro et al., 2017, 2018). Scleractinian corals carpets (*Retiophillia* sp.) also occur in this unit (Todaro et al., 2017).

In Unit B the scleractinian corals and the dicerocardids disappear and the bivalve community is represented only by small specimens of *Neomegalodon* and *Triadomegalodon* sp., the size of which does not exceed 10–15 cm (Todaro et al., 2018) (**Figure 2A, B, C**). The top of Unit B corresponds to the last occurrence (LO) of *T. hantkeni* and megalodontoids and to the presence of a discontinuous level up to 20 cm thick consisting of oolitic grainstone and interpreted as a storm layer (**Figure 3D**). A 10 m thick barren zone dominated by calcitic sphaerules (up to 200 µm in diameter) separates Unit B from Unit C (**Figure 3E**). In the subtidal facies of Unit C the fossil content consists almost exclusively by the encrusting alga *Thaumatoporella parvovesiculifera* associated with rare *Aeolisaccus dunningtoni* (**Figure 3F**). Upsection, the first benthic foraminifer *Siphovalvulina* sp. occurs about 10 m above the base of Unit C.

ISOTOPIC DATA

CAMP Influence (Sr, Zn, Pb)

The newly determined $^{87}Sr/^{86}Sr$ values of the Mt Sparagio section range between ~0.7075 and ~0.7087 (**Figure 4**), with the greatest majority of them overlapping the end-Triassic seawater composition ~0.70771-0.70776 (McArthur et al., 2001). Only six samples deviate significantly from the end-Triassic seawater composition (**Figure 4**). Two samples at the base of Unit B (Z15 and Z23) have less radiogenic Sr isotope compositions than seawater, overlapping with the compositional field of CAMP. The sample (Z18) that is stratigraphically comprised between these two samples shows an end-Triassic seawater Sr composition. In Unit C three samples have significantly more radiogenic $^{87}Sr/^{86}Sr$ values than end-Triassic seawater (TJ45, TJ48, TJ56), and are intercalated in the stratigraphic section by a sample (TJ54) with a $^{87}Sr/^{86}Sr$ value less radiogenic than end-Triassic seawater, shifted towards the CAMP isotope composition. The topmost sample of the investigated section (TJ58) is also slightly less radiogenic than end-Triassic seawater.

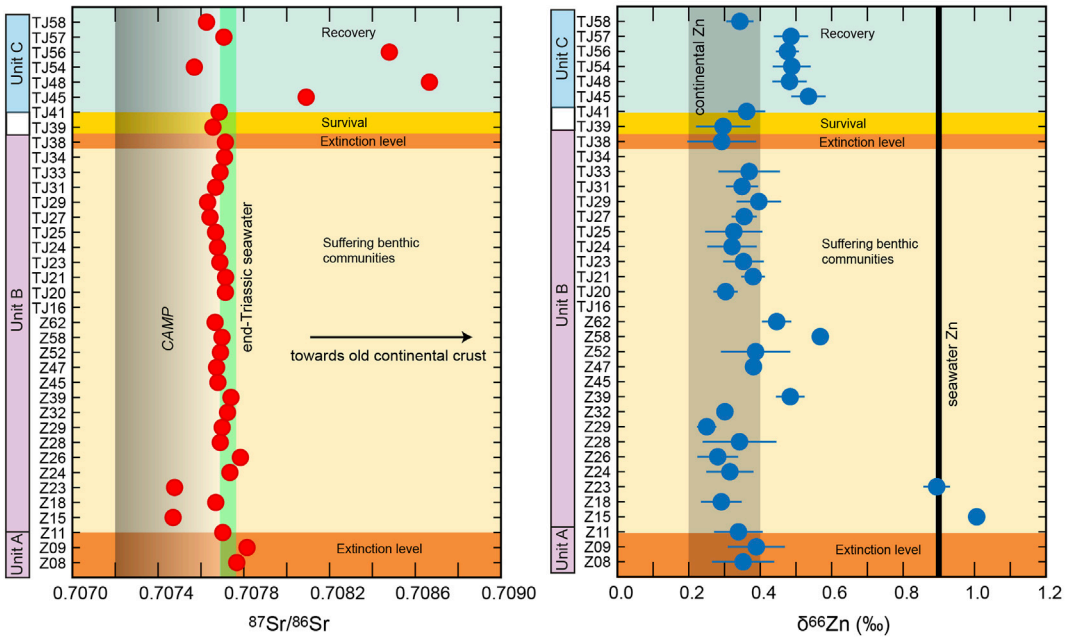

FIGURE 4 | $^{87}Sr/^{86}Sr$ values and $\delta^{66}Zn$ values of the Mt Sparagio section correlated to the three Units and to the extinction events (not in scale).

The $\delta^{66}Zn$ values of the Mt Sparagio section range between +0.25 and +1.00‰ (**Figure 4**). The greatest majority of them fall in the isotopic compositional range (~+0.3 to +0.4‰) of continental rocks and riverine input (Chen et al., 2013; Little et al., 2014). At the base of Unit B, two samples (Z15 and Z23) with CAMP-like Sr isotope compositions are characterized by $\delta^{66}Zn$ values between +0.9 and +1.0‰, similar to modern surface seawater (Maréchal et al., 2000; Little et al., 2014). Sample Z18, stratigraphically comprised between Z15 and Z23, which is characterized by an end-Triassic seawater Sr composition, has a continental Zn isotope signature. Therefore, the three samples in this part of the section show an anti-correlation between Sr and Zn isotope compositions. Three samples (Z39, Z58, Z62) in the middle part of the Unit B display erratic spikes marginally ($\delta^{66}Zn$ values of +0.45 and +0.48‰) to significantly heavier ($\delta^{66}Zn$ ~+0.58‰) than the dominant continental Zn recorded by the bulk of the section. The Unit C is characterized by a package of five stratigraphically sequential samples that show slightly but consistently higher $\delta^{66}Zn$ values (~+0.48 to +0.54‰) with respect to the continental Zn isotope range. This interval of the section corresponds to the samples that have either significantly more or slightly less radiogenic Sr than end-Triassic seawater. The topmost levels of Unit C returns to a continental Zn isotope signature.

Because of the very low concentrations of Pb in the investigated samples, only six of them returned reliable results (i.e., not affected by poor uncertainty and large uncontrolled instrumental mass fractionation due to low counting statistics). Two samples are those from the base of the section which returned CAMP-like Sr isotope compositions, two are from the middle part of the section with an end-Triassic seawater Sr isotope composition, and two are from the upper part of the section with a highly radiogenic Sr isotope composition (**Figure 5**). Initial isotope ratios of $^{206}Pb/^{204}Pb$, $^{207}Pb/^{204}Pb$ and $^{208}Pb/^{204}Pb$, corrected for time-integrated decay of U (and Th) at 200 Ma using U/Pb (and Th/Pb) ratios of Mesozoic Sicilian carbonates of comparable environment, are comprised between 18.27-23.21, 15.62-15.86, 38.15-38.82, respectively. The samples with CAMP-like Sr isotope compositions from the base of the section and those from the middle part of the section returned Pb isotope compositions consistent with CAMP (**Figure 5**). The samples from the upper part of the section, which have the most radiogenic $^{87}Sr/^{86}Sr$ values, have also the most radiogenic Pb isotope composition (outside CAMP), with high $^{207}Pb/^{204}Pb$ values that are indicative of derivation from relatively old continental rocks with high μ ($^{238}U/^{204}Pb$) values (**Figure 5**).

C,O and S

The new Sr and Zn isotope results are integrated with previously obtained C, O (Todaro et al., 2018) and S (He et al., 2020) isotope curves in **Figure 6**. The $\delta^{13}C_{carb}$ curve shows two main negative excursions separated by a positive peak with values ranging from -2.58‰ to 3.03‰ close to the base of the studied section (Todaro et al., 2018). The first negative trend shows a rapid decrease from ca. +1‰ to −2‰ at the top of Unit A followed by a return to more positive values up to +3‰. The second negative trend shows a decrease to more negative values of about −2.5‰ along the Unit B. After the second negative excursion, the carbon curve shows a gradual return to more positive values up to ca. +2.5‰ along Unit C (**Figure 6**).

The $\delta^{18}O_{carb}$ values were used to assess a possible climate change around the TJB (Todaro et al., 2018). At the top of Unit A,

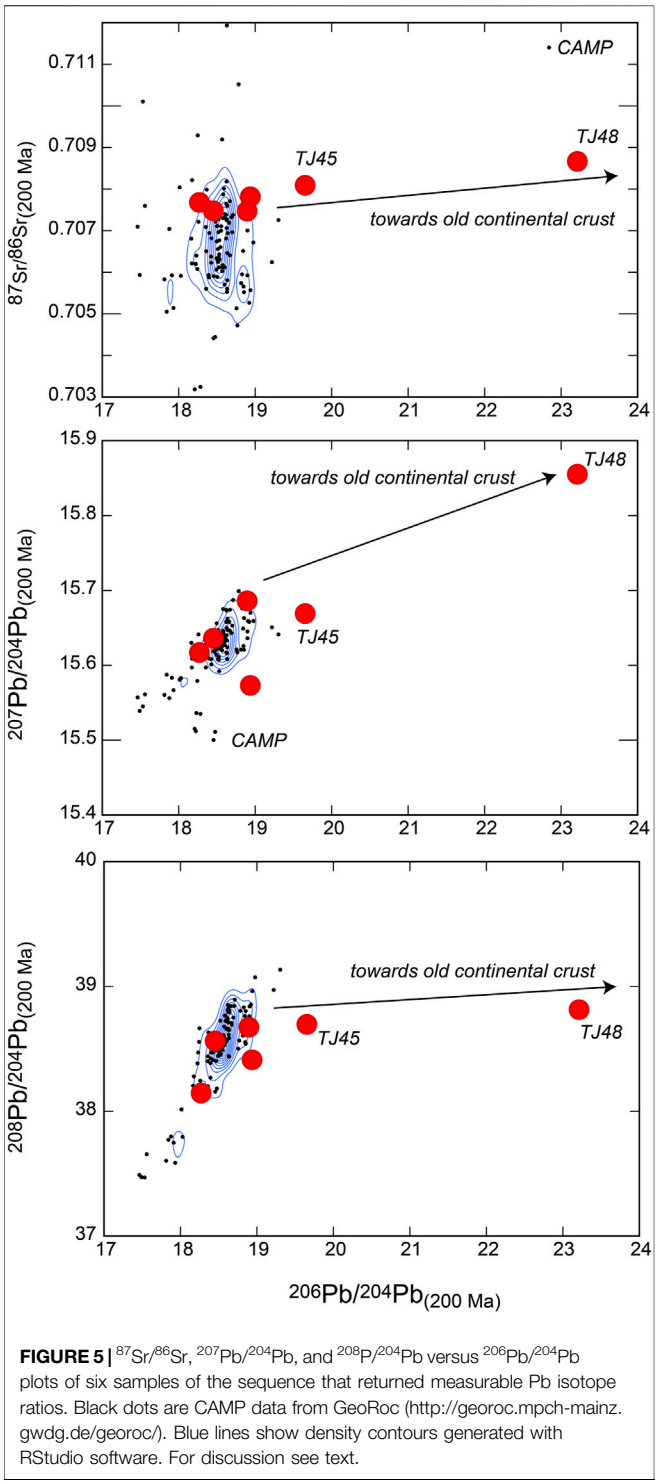

FIGURE 5 | $^{87}Sr/^{86}Sr$, $^{207}Pb/^{204}Pb$, and $^{208}P/^{204}Pb$ versus $^{206}Pb/^{204}Pb$ plots of six samples of the sequence that returned measurable Pb isotope ratios. Black dots are CAMP data from GeoRoc (http://georoc.mpch-mainz.gwdg.de/georoc/). Blue lines show density contours generated with RStudio software. For discussion see text.

the first warming trend (low $\delta^{18}O_{carb}$ values) is followed by a short cooling interval and then by a second more prolonged warming trend along the Unit B. A positive $\delta^{18}O_{carb}$ shift, at the TJB, crossing the interval between Unit B and Unit C, suggests instead the end of the warming phase (**Figure 6**).

The $\delta^{34}S_{CAS}$ curve shows a stable trend except for a large positive shift with a magnitude of >10‰ recorded at the top of Unit B (He et al., 2020) and coincident with the extinction of the Triassic benthic community (**Figure 6**).

DISCUSSION

The Mt Sparagio section offers at present the most complete record of the biostratigraphic and chemostratigraphic variations across the TJB in a continuous shallow water setting. Biostratigraphically, the Mt. Sparagio is easily comparable to other shallow water section described from the western Tethys, such as Croci di Acierno (Southern Apennines, De Castro 1990), Mt Messapion (Greece, Romano et al., 2008), Tahtaiskele (Karaburun Peninsula Turkey, Tunaboylu et al., 2014) and Mt Cefalo (Southern Apennines, Bachan et al., 2012), where similar extinction and recovery patterns of microfossil associations are described. As far as concern the macrofossil associations, in many of the Tethyan sections the presence of gigantic specimens of megalodontoids in the Rhaetian beds is reported by several authors (Végh-Neubrandt, 1982; Allasinaz, 1992, among others). The huge shell size reached by these pelecypods is attributed to the presence of photosymbionts (Végh-Neubrandt, 1982; De Freitas et al., 1993) as occurred in the Wallowaconchidae during the Upper Triassic of western North America (Yancey and Stanley, 1999), and their reduction in size has been attributed to the cessation of this symbiotic partnership (van de Schootbrugge and Wignall, 2016). At Mt Sparagio, the megalodontoids extinction trend shows two main pulses during the Rhaetian as high-diverse and giant species are confined to Unit A, while only few and small species are present in overlying Unit B, before the total extinction recorded in Unit C. The factors that controlled the reduction in biodiversity and size seem to have played a little role on the Rhaetian foraminifer association, except for the foraminifer *Triasina hantkeni* that recorded a diameter reduction between Unit A and B (Todaro et al., 2017).

The two extinction pulses recorded by the bivalve community are strictly correlated with the environmental perturbations documented as variation trends of the isotopic curves. In particular, the two pulses match well with the two $\delta^{13}C_{carb}$ negative excursions (**Figure 6**). The link between carbon isotope variations in the sedimentary record (Schobben et al., 2019) and mass extinction events (Raup and Sepkoski Jr, 1982) has typically been interpreted as caused by perturbations in the geological carbon cycle (Suarez et al., 2019) due to massive injection of isotopically light C, the ultimate effects of which would be global warming, oceanic acidification and a decrease of available carbonate in marine waters. Although the origin of this C is still debated (Suarez et al., 2019), there is now documented evidence (Wignall, 2001) for a likely role played by a surge of volcanic gas emissions during the emplacement of Large Igneous Provinces (LIP), including the CAMP that occurred right at the TJB (Hautmann et al., 2008; Greene et al., 2012; McRoberts et al., 2012; Al-Suwaidi et al., 2016). This interpretation of a LIP trigger has traditionally been hampered by the lack of sufficient information on the CO_2 abundance in these magmas (Black and Gibson, 2019). However, there is growing evidence that CAMP magmas may have been CO_2-rich (Capriolo et al.,

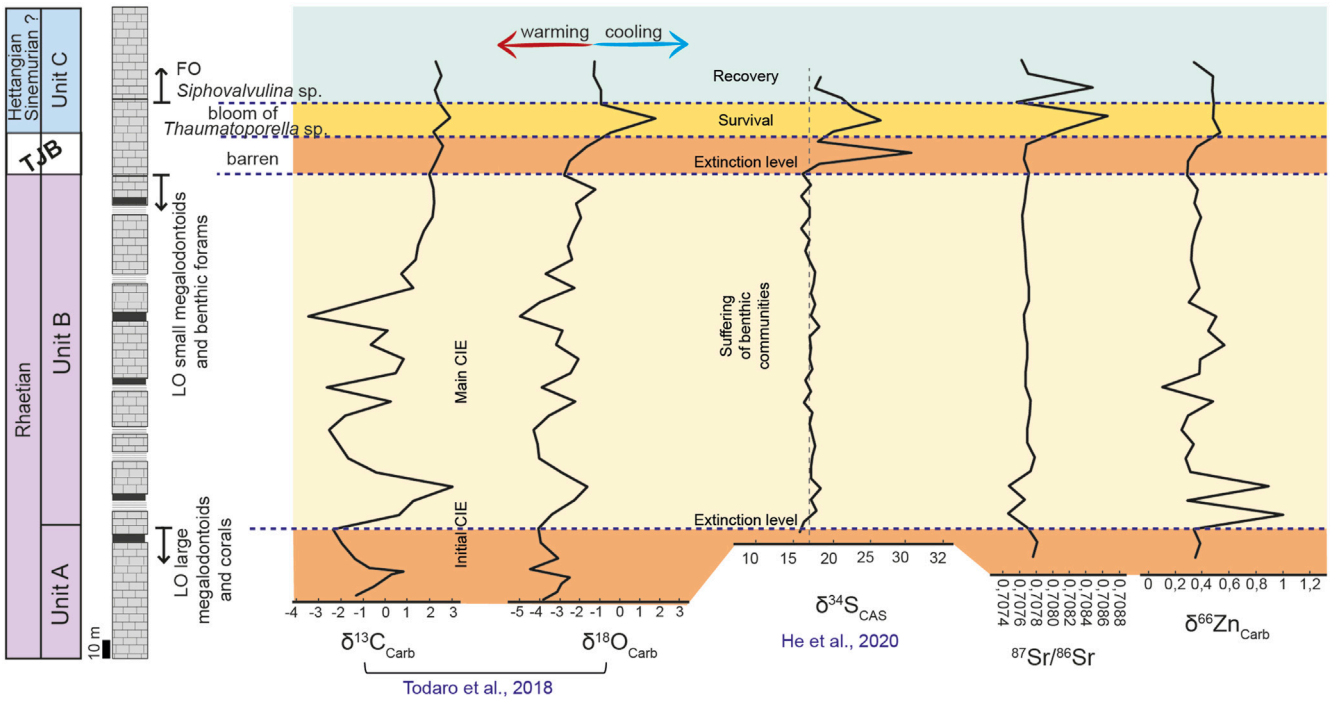

FIGURE 6 | Isotopic curves obtained in the Mt Sparagio section. The trends of the curves indicate environmental perturbations (acidification, climatic changes, marine anoxia, CAMP-influence) correlated with the two extinction pulses of the benthic community in the Rhaetian horizons. Black intervals represent the supratidal members of the peritidal cycles. The $\delta^{13}C_{carb}$ and $\delta^{18}O_{carb}$ are illustrated in Todaro et al. (2018), the $\delta^{34}S_{CAS}$ curve is after He et al. (2020).

2021), and modern volcano analogues (Aiuppa et al., 2021) indicate that magmas in rift and ocean island environments, can transport potentially large quantities of carbon to potentially trigger environmental change upon atmospheric injection if sourced deep in the upper mantle. In addition to perturbation of the carbon cycle, a temperature increase was also attributed to the CAMP activity (McElwain et al., 1999; Lindström et al., 2017). This is also well observable in the Mt Sparagio section by the trend of the $\delta^{18}O_{carb}$ curve (**Figure 6**). In particular, the biocalcification crisis characterized by a reduction of megalodontoids biodiversity seems strongly related to warmer temperatures recorded by low $\delta^{18}O_{carb}$ values while the end of this warming phase is marked by a positive $\delta^{18}O_{carb}$ shift and correlated to the extinction of the Rhaetian benthic community (Todaro et al., 2018). Warming and CO_2-induced ocean acidification are likely to have resulted eventually in oceanic anoxia, as fully supported by $\delta^{34}S_{CAS}$ curve (**Figure 6**). This exhibits a stable trend that is interrupted by a positive peak in correspondence of the extinction of Rhaetian benthic community, suggestive of the onset of anoxic conditions. The persistence of the positive trend throughout the barren interval suggests that anoxic conditions prevailed over the entire TJB interval (He et al., 2020).

Clues From Zn, Sr and Pb Isotopes

Zn isotopes are increasingly used to better understand processes related with mass extinctions and following biological recovery (Kunzmann et al., 2013; Liu et al., 2017). This opportunity is favoured by the Zn isotope compositions of seawater being significantly heavier than those of magmatic rocks and riverine input into oceans ($\delta^{66}Zn$ ~0.2–0.4‰: Chen et al., 2013; Little et al., 2014; **Figure 4**). The heavier Zn isotope composition of seawater is due to the preferential uptake of light Zn (^{64}Zn) by phytoplankton (using Zn as a micronutrient), resulting in a relative increase of the heavier Zn isotopes (e.g., ^{66}Zn) and therefore in higher $\delta^{66}Zn$ values in seawater (Marechal et al., 2000).

Similarly to Sr (Veizer, 1989), Zn in carbonates can derive either from dissolved Zn in seawater (from which carbonates chemically precipitate) or from continental Zn (if carbonates contain a detrital clay component) (Liu et al., 2017). The combined use of Sr and Zn isotopes in the same rock sample can therefore help better resolving seawater vs detrital origins for elements (**Figure 7**). Most of the samples in the investigated section show Sr isotope compositions consistent with that of end-Triassic seawater (**Figure 7**). This observation argues against a major detrital contribution from the continents, suggesting that the Zn isotope composition of the samples should also reflect the composition of seawater. However, the Zn isotopic signature of the largest part of the sequence is typical of riverine input and magmatic rocks, especially in the median-upper part of Unit B and in the barren interval (**Figures 4**, **6**), suggesting that the biological activity was strongly to completely suppressed in the greatest part of the investigated section. In fact, biological activity should drive the dissolved Zn introduced into seawater by riverine input magmatic activity with initial

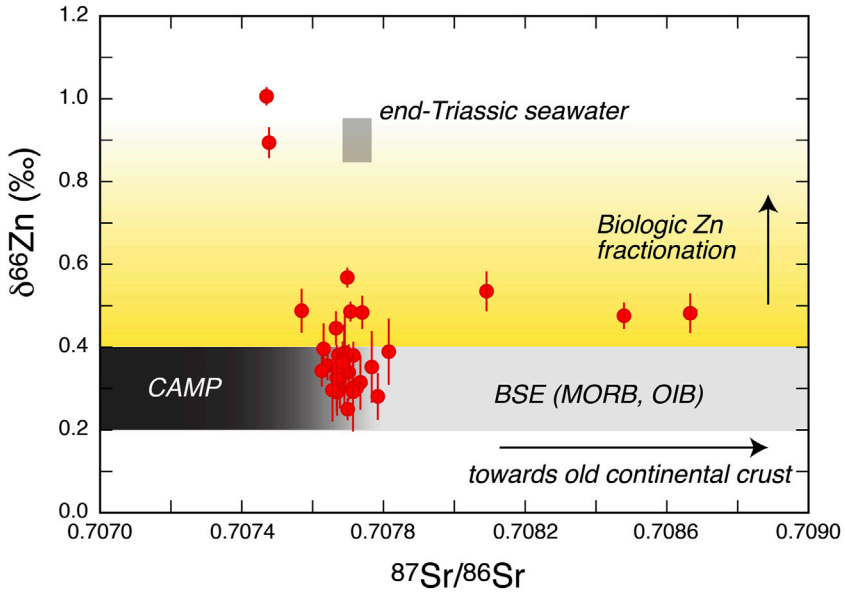

FIGURE 7 | Combined graph of Sr and Zn for the Mt Sparagio section used to resolve seawater vs detrital origins for elements. The end-Triassic (201–201.5 Ma) Sr seawater composition is from McArthur et al. (2001).

δ^{66}Zn ~0.2–0.4‰ to heavier isotope composition because of preferential uptake of light Zn by phytoplankton. Our data therefore support the use of Zn isotopes to track biological crises in the sedimentary record during pre- and syn-extinction levels, as also documented in the end-Permian mass extinction (Liu et al., 2017).

In contrast to this behaviour, at the base of Unit B (samples Z15 and Z23), Sr and Zn isotopes exhibit some peculiar signature (**Figures 4**, **6**). In this part of the section, the least radiogenic Sr isotope compositions are observed, and are associated with the most positive δ^{66}Zn compositions in our dataset (**Figures 4**, **6**, **7**). We stress that, as no petrographic evidence has been found for secondary/diagenetic processes, these Sr-Zn isotope signature must reflect sin-depositional processes. Moreover, the unusually low radiogenic $^{87}Sr/^{86}Sr$ signatures combined with Pb isotopes (**Figure 5**) overlap with the compositional field of CAMP volcanism. We thus propose that these isotopic compositions likely reflect a dominant and local input of "detrital" Sr derived from CAMP, either in the form of eroded particulate materials or volcanic fallout. The proximity of this CAMP-related Sr input is supported by the fact that seawater Sr isotope compositions are thought to be rapidly (within the timescales of the sedimentary record) homogenized throughout all oceans (Veizer, 1989). A local input also fits with the low Pb residence time in seawater.

The corresponding heavy (**Figure 7**) Zn isotope compositions (δ^{66}Zn of +0.9 and +1.0‰) are more puzzling to interpret. One possibility is that they reflect episodic and short events of increased biological activity, perhaps related to transient increased ocean productivity caused by micro-nutrient input during CAMP volcanism. Elevated volcanic nutrient supplies, perhaps related to oceanic deposition of volcanic ash (Jones and Gislason, 2008), have been recently suggested as drivers for the late Ordovician extinctions (Longman et al., 2021). However, this interpretation clashes with the evidence of detrital Sr at the base Unit B (samples Z15 and Z23). Since CAMP material contains several tens of ppm Zn, whereas seawater Zn concentrations are <1 ppb, it seems unlikely that the incorporation of "detrital" CAMP material (suggested by Sr isotopes) would have not resulted into a continental Zn isotopic signature (i.e., δ^{66}Zn +0.2–0.4‰) for these samples. A possible explanation is that there is a decoupling between Sr and Zn during the precipitation of carbonate rocks, in which the Zn would be more sensible to biological (rather than detrital) drivers. We finally note that the unusual composition of these two samples does not affect the general interpretation, discussed above, of the bulk sequence representing conditions of suppressed biological activity.

The top part of the sequence also shows some peculiar isotope compositions in Unit C, where an unusually radiogenic Sr (Figs., 4, 5, 6) and Pb (**Figure 5**) signature is observed. These compositions reveal a clear input of non-seawater, detrital Sr (and Pb) at the top of the sequence, with the radiogenic Sr and Pb signatures implying an old continental crustal source. We propose that this crustal contribution was derived from weathering of Variscan Calabrian-Peloritan Orogen (Fiannacca et al., 2019).

Interestingly, the samples belonging to Unit C exhibit a consistent Zn isotope signature that is slightly heavier than that of continental zinc (**Figures 6**, **7**), suggesting that the input from a more proximal continental crust basement was associated with the onset of a renewed biological activity and

consistent with the recovery phase of the Lower Jurassic carbonate factory.

CONCLUSION

The present study aimed to highlight a tight relationship between the environmental variations inferred by the isotopic records and the ETE pulses recorded by the Mt Sparagio section.

In the studied section, the isotope data of C, O, and S are indicative of serious environmental variations as recorded worldwide and related to the CAMP activity. The two negative excursions documented by the C-curve (Initial-CIE and Main-CIE) confirm the acidification processes that involved the benthic community. Moreover, the climate variations estimated from the oxygen isotopes indicate a warming-trend that corresponds to the reduction in biodiversity and size of the megalodontoids in the upper part of the Rhaetian beds. This warming trend could have deteriorated the photosymbiotic relationships of these pelecypods as inferred by several authors to explain their gigantism.

In the studied section, the total extinction of the Rhaetian benthic association is clearly related to a long-lasting carbon negative excursion (Main-CIE) coupled to a further warming trend.

Although the influence of CAMP on the ETE is well described in many TJB sections, the new isotope data (Zn, Pb, Sr) from Mt Sparagio section offer substantial documentation of a tight control of the Large Igneous Provinces on mass extinction events.

DATA AVAILABILITY STATEMENT

The original contributions presented in the study are included in the article/**Supplementary Material**, further inquiries can be directed to the corresponding author.

AUTHOR CONTRIBUTIONS

Field survey and data acquisition (ST; MR; PDS). Data interpretations (ST; MR; PDS; MC, AA). Writing- original draft (ST; MR; MC). Writing editing (ST; MR; PDS; MC; AA). Writing review (ST; MR; PDS; MC; AA). Illustrations (ST; MC).

FUNDING

This work was carried out with the financial support of the University of Palermo (2019_AIM_CTC_DISTEM_CI_1) by ST, (R4D14-P5F5RISS-MARGINE) by PDS and University of Padova (DOR1978195/19) by MR. AA acknowledges funding from the Italian Ministero Istruzione Università e Ricerca (Miur, Grant No. 2017LMNLAW).

SUPPLEMENTARY MATERIAL

The Supplementary Material for this article can be found online at: https://www.frontiersin.org/articles/10.3389/feart.2022.875466/full#supplementary-material

Supplementary Table S1 | Facies types and environmental interpretation described in the Mt Sparagio section (modified after Todaro et al., 2017).

REFERENCES

Abate, B., Di Maggio, C., Incandela, A., and Renda, P. (1991). Nuovi dati sulla geologia della Penisola di Capo San Vito (Sicilia nord-occidentale). *Mem. Della Soc. Geol. Ital.* 47, 15–25.

Aiuppa, A., Casetta, F., Coltorti, M., Stagno, V., and Tamburello, G. (2021). Carbon Concentration Increases with Depth of Melting in Earth's Upper Mantle. *Nat. Geosci.* 14, 697–703. doi:10.1038/s41561-021-00797-y

Al-Suwaidi, A. H., Steuber, T., and Suarez, M. B. (2016). The Triassic-Jurassic Boundary Event from an Equatorial Carbonate Platform (Ghalilah Formation, United Arab Emirates). *J. Geol. Soc.* 173, 949–953. doi:10.1144/jgs2015-102

Allasinaz, A. (1992). The Late Triassic-Hettangian Bivalves Turnover in Lombardy (Southern Alps) Verlag Nicht Ermittelbar. *Riv. It. Paleont. Strat.* 97, 431–454.

Antonelli, M., Franciosi, R., Pezzi, G., Querci, A., Ronco, G. P., and Vezzani, F. (1988). Paleogeographic Evolution and Structural Setting of the Northern Side of the Sicily Channel. *Mem. Della Soc. Geol. Ital.* 41, 141–157. doi:10.1016/0304-3800(88)90029-4

Bachan, A., Van De Schootbrugge, B., Fiebig, J., McRoberts, C. A., Ciarapica, G., and Payne, J. L. (2012). Carbon Cycle Dynamics Following the End-Triassic Mass Extinction: Constraints from pairedδ13Ccarbandδ13Corgrecords. *Geochem. Geophys. Geosyst.* 13, 415. doi:10.1029/2012GC004150

Barattolo, F., and Romano, R. (2005). Shallow Carbonate Platform Bioevents during the Upper Triassic-Lower Jurassic: an Evolutive Interpretation. *Boll. Della Soc. Geol. Ital.* 124, 123–142.

Beerling, D. J., and Berner, R. A. (2002). Biogeochemical Constraints on the Triassic-Jurassic Boundary Carbon Cycle Event. *Glob. Biogeochem. Cycles* 16, 10–13. doi:10.1029/2001GB001637

Black, B. A., and Gibson, S. A. (2019). Deep Carbon and the Life Cycle of Large Igneous Provinces. *Elements* 15, 319–324. doi:10.2138/gselements.15.5.319

Blackburn, T. J., Olsen, P. E., Bowring, S. A., McLean, N. M., Kent, D. V., Puffer, J., et al. (2013). Zircon U-Pb Geochronology Links the End-Triassic Extinction with the Central Atlantic Magmatic Province. *Science* 340, 941–945. doi:10.1126/science.1234204

Cacciatore, M. S., Todaro, S., Zarcone, G., and Di Stefano, P. (2010). Triasina Hantkeni Limestones from Western SicilyNew Developments on Triassic Integrated Stratigraphy. *Albertiana* 39, 87.

Callegaro, S., Rapaille, C., Marzoli, A., Bertrand, H., Chiaradia, M., Reisberg, L., et al. (2014). Enriched Mantle Source for the Central Atlantic Magmatic Province: New Supporting Evidence from Southwestern Europe. *Lithos* 188, 15–32. doi:10.1016/j.lithos.2013.10.021

Capriolo, M., Mills, B. J. W., Newton, R. J., Dal Corso, J., Dunhill, A. M., Wignall, P. B., et al. (202210373). Anthropogenic-scale CO2 Degassing from the Central Atlantic Magmatic Province as a Driver of the End-Triassic Mass Extinction. *Glob. Planet. Change* 209, 103731. doi:10.1016/j.gloplacha.2021.103731

Catalano, R., Doglioni, C., and Merlini, S. (2001). On the Mesozoic Ionian basin. *Geophys. J. Int.* 144, 49–64. doi:10.1046/j.0956-540x.2000.01287.x

Chen, H., Savage, P. S., Teng, F.-Z., Helz, R. T., and Moynier, F. (2013). Zinc Isotope Fractionation during Magmatic Differentiation and the Isotopic Composition of the Bulk Earth. *Earth Planet. Sci. Lett.* 369-370, 34–42. doi:10.1016/j.epsl.2013.02.037

Chiaradia, M., Müntener, O., and Beate, B. (2020). Effects of Aseismic ridge Subduction on the Geochemistry of Frontal Arc Magmas. *Earth Planet. Sci. Lett.* 531, 115984. doi:10.1016/j.epsl.2019.115984

Chiaradia, M., Pujol-Solà, N., Farré-de-Pablo, J., Aiuppa, A., Paonita, A., Rizzo, A. L., et al. (2018). Geochemistry and Isotope Composition (Sr, Pb, δ66Zn) of

Vulcano Fumaroles (Aeolian Islands, Italy). *Chem. Geology.* 493, 153–171. doi:10.1016/j.chemgeo.2018.05.038

Chiocchini, M., Farinacci, A., Mancinelli, A., Molinari, V., and Potetti, M. (1994). Biostratigrafia a foraminiferi, dasicladali e calpionelle delle successioni carbonatiche mesozoiche dell'Appennino centrale (Italia). *Biostratigrafia dell'Italia Centrale.* 9–129. doi:10.15165/studgeocam-1128

Ciarapica, G. (2007). Regional and Global Changes Around the Triassic-Jurassic Boundary Reflected in the Late Norian-Hettangian History of the Apennine Basins. *Palaeogeogr. Palaeoclimatol. Palaeoecol.* 244, 34–51. doi:10.1016/j.palaeo.2006.06.022

Coskun Tunaboylu, B., Altiner, D., İsintek, İ., and Demirci, D. (2014). Foraminiferal Biostratigraphy and Sequence Stratigraphy of Peritidal Carbonates at the Triassic-Jurassic Boundary (Karaburun Peninsula, Western Turkey). *J. Asian Earth Sci.* 90, 61–76. doi:10.1016/j.jseaes.2014.04.015

Davies, J. H. F. L., Marzoli, A., Bertrand, H., Youbi, N., Ernesto, M., and Schaltegger, U. (2017). End-Triassic Mass Extinction Started by Intrusive CAMP Activity. *Nat. Commun.* 8, 1–8. doi:10.1038/ncomms15596

De Castro, P. (1990). Studies on the Triassic Carbonates of the Salerno Province (Southern Italy): the Croci d'Acerno Sequence. *Boll. Della Soc. Geol. Ital.* 109, 187–217.

De Freitas, T. A., Brunton, F., and Bernecker, T. (1993). Silurian Megalodont Bivalves of the Canadian Arctic and Australia: Paleoecology and Evolutionary Significance. *Palaios* 8, 450–464. doi:10.2307/3515019

Deenen, M. H. L., Ruhl, M., Bonis, N. R., Krijgsman, W., Kuerschner, W. M., Reitsma, M., et al. (2010). A New Chronology for the End-Triassic Mass Extinction. *Earth Planet. Sci. Lett.* 291, 113–125. doi:10.1016/j.epsl.2010.01.003

Di Bari, D., and Rettori, R. (1996). Morphological Features of Triasina Hantkeni Majzon, 1954 (Foraminiferida, Aulotortidae) and Remarks on the Test wall Structure. *Revue de Micropaléontologie* 39, 305–313. doi:10.1016/S0035-1598(96)90146-4

Di Stefano, P., Favara, R., Luzio, D., Renda, P., Cacciatore, M. S., Calò, M., et al. (2015). A Regional-Scale Discontinuity in Western Sicily Revealed by a Multidisciplinary Approach: A New Piece for Understanding the Geodynamic Puzzle of the Southern Mediterranean. *Tectonics* 34, 2067–2085. doi:10.1002/2014TC003759

Fiannacca, P., Williams, I. S., Cirrincione, R., and Pezzino, A. (2019). Poly-orogenic Melting of Metasedimentary Crust from a Granite Geochemistry and Inherited Zircon Perspective (Southern Calabria-Peloritani Orogen, Italy). *Front. Earth Sci.* 7, 119. doi:10.3389/feart.2019.00119

Finetti, I. R., Del Ben, A., Fais, S., Forlin, E., Klingelé, E., Lecca, L., et al. (2005). "Crustal Tectono-Stratigraphic Setting of the Pelagian Foreland from the New CROP Seismic Data," in *CROP Project - Deep Seismic Explanation of the Central Mediterranean and Italy*, 413–446.

Galli, M. T., Jadoul, F., Bernasconi, S. M., Cirilli, S., and Weissert, H. (2007). Stratigraphy and Palaeoenvironmental Analysis of the Triassic-Jurassic Transition in the Western Southern Alps (Northern Italy). *Palaeogeogr. Palaeoclimatol. Palaeoecol.* 244, 52–70. doi:10.1016/j.palaeo.2006.06.023

Gazdzicki, A. (1983). Foraminifers and Biostratigraphy of Upper Triassic and Lower Jurassic of the Slovakian and Polish Carpathians. *Palaeontol. Pol.* 44, 109–169.

Giunta, G., and Liguori, V. (1972). La Geologia Dell'estremità Nord-Occidentale Della Sicilia. *Riv. Min. Sic.* 23 , 136–138, 165–226.

Greene, S. E., Martindale, R. C., Ritterbush, K. A., Bottjer, D. J., Corsetti, F. A., and Berelson, W. M. (2012). Recognising Ocean Acidification in Deep Time: An Evaluation of the Evidence for Acidification across the Triassic-Jurassic Boundary. *Earth-Science Rev.* 113, 72–93. doi:10.1016/j.earscirev.2012.03.009

Guex, J., Bartolini, A., Atudorei, V., and Taylor, D. (2004). High-resolution Ammonite and Carbon Isotope Stratigraphy across the Triassic-Jurassic Boundary at New York Canyon (Nevada). *Earth Planet. Sci. Lett.* 225, 29–41. doi:10.1016/j.epsl.2004.06.006

Hallam, A. (1997). Estimates of the Amount and Rate of Sea-Level Change across the Rhaetian-Hettangian and Pliensbachian-Toarcian Boundaries (Latest Triassic to Early Jurassic). *J. Geol. Soc.* 154, 773–779. doi:10.1144/gsjgs.154.5.077310.1144/gsjgs.154.5.0773

Hautmann, M., Benton, M. J., and Tomašových, A. (2008). Catastrophic Ocean Acidification at the Triassic-Jurassic Boundary. *njgpa* 249, 119–127. doi:10.1127/0077-7749/2008/0249-0119

He, T., Dal Corso, J., Newton, R. J., Wignall, P. B., Mills, B. J. W., Todaro, S., et al. (2020). An Enormous Sulfur Isotope Excursion Indicates marine Anoxia during the End-Triassic Mass Extinction. *Sci. Adv.* 6, eabb6704. doi:10.1126/sciadv.abb6704

He, T., Newton, R. J., Wignall, P. B., Reid, S., Dal Corso, J., Takahashi, S., et al. (2022). Shallow Ocean Oxygen Decline during the End-Triassic Mass Extinction. *Glob. Planet. Change* 210, 103770. doi:10.1016/j.gloplacha.2022.103770

Hesselbo, S. P., Robinson, S. A., Surlyk, F., and Piasecki, S. (2002). Terrestrial and marine Extinction at the Triassic-Jurassic Boundary Synchronized with Major Carbon-Cycle Perturbation: A Link to Initiation of Massive Volcanism? *Geol* 30, 251–254. doi:10.1130/0091-7613(2002)030<0251:tameat>2.0.co;2

Huynh, T. T., and Poulsen, C. J. (2005). Rising Atmospheric CO2 as a Possible Trigger for the End-Triassic Mass Extinction. *Palaeogeogr. Palaeoclimatol. Palaeoecol.* 217, 223–242. doi:10.1016/j.palaeo.2004.12.004

Jones, M. T., and Gislason, S. R. (2008). Rapid Releases of Metal Salts and Nutrients Following the Deposition of Volcanic Ash into Aqueous Environments. *Geochimica et Cosmochimica Acta* 72, 3661–3680. doi:10.1016/j.gca.2008.05.030

Jost, A. B., Bachan, A., van De Schootbrugge, B., Lau, K. V., Weaver, K. L., Maher, K., et al. (2017). Uranium Isotope Evidence for an Expansion of marine Anoxia during the End- T Riassic Extinction. *Geochem. Geophys. Geosyst.* 18, 3093–3108. doi:10.1002/2017GC006941

Kamoun, F., Peybernès, B., Ciszak, R., and Calzada, S. (2001). Triassic Palaeogeography of Tunisia. *Palaeogeogr. Palaeoclimatol. Palaeoecol.* 172, 223–242. doi:10.1016/S0031-0182(01)00283-8

Kiessling, W., Aberhan, M., Brenneis, B., and Wagner, P. J. (2007). Extinction Trajectories of Benthic Organisms across the Triassic-Jurassic Boundary. *Palaeogeogr. Palaeoclimatol. Palaeoecol.* 244, 201–222. doi:10.1016/j.palaeo.2006.06.029

Kunzmann, M., Halverson, G. P., Sossi, P. A., Raub, T. D., Payne, J. L., and Kirby, J. (2013). Zn Isotope Evidence for Immediate Resumption of Primary Productivity after Snowball Earth. *Geology* 41, 27–30. doi:10.1130/G33422.1

Larina, E., Bottjer, D. J., Corsetti, F. A., Thibodeau, A. M., Berelson, W. M., West, A. J., et al. (2021). Ecosystem Change and Carbon Cycle Perturbation Preceded the End-Triassic Mass Extinction. *Earth Planet. Sci. Lett.* 576, 117180. doi:10.1016/j.epsl.2021.117180

Lindström, S. (2016). Palynofloral Patterns of Terrestrial Ecosystem Change during the End-Triassic Event - A Review. *Geol. Mag.* 153, 223–251. doi:10.1017/S0016756815000552

Lindström, S. (2021). Two-phased Mass Rarity and Extinction in Land Plants during the End-Triassic Climate Crisis. *Front. Earth Sci.* 9, 343. doi:10.3389/feart.2021.780343

Lindström, S., van de Schootbrugge, B., Hansen, K. H., Pedersen, G. K., Alsen, P., Thibault, N., et al. (2017). A New Correlation of Triassic-Jurassic Boundary Successions in NW Europe, Nevada and Peru, and the Central Atlantic Magmatic Province: A Time-Line for the End-Triassic Mass Extinction. *Palaeogeogr. Palaeoclimatol. Palaeoecol.* 478, 80–102. doi:10.1016/j.palaeo.2016.12.025

Little, S. H., Vance, D., Walker-Brown, C., and Landing, W. M. (2014). The Oceanic Mass Balance of Copper and Zinc Isotopes, Investigated by Analysis of Their Inputs, and Outputs to Ferromanganese Oxide Sediments. *Geochimica et Cosmochimica Acta* 125, 673–693. doi:10.1016/j.gca.2013.07.046

Liu, S.-A., Wu, H., Shen, S.-z., Jiang, G., Zhang, S., Lv, Y., et al. (2017). Zinc Isotope Evidence for Intensive Magmatism Immediately before the End-Permian Mass Extinction. *Geology* 45, 343–346. doi:10.1130/G38644.1

Lo Cicero, G. (1986). Carbon and Oxygen Isotopic Composition of Norian Sediments. Panormide Carbonate Platform, Palermo. *Rend. Soc. Geol. It.* 9, 209–218.

Longman, J., Mills, B. J. W., Manners, H. R., Gernon, T. M., and Palmer, M. R. (2021). Late Ordovician Climate Change and Extinctions Driven by Elevated Volcanic Nutrient Supply. *Nat. Geosci.* 14, 924–929. doi:10.1038/s41561-021-00855-5

Luo, G., Richoz, S., van de Schootbrugge, B., Algeo, T. J., Xie, S., Ono, S., et al. (2018). Multiple Sulfur-Isotopic Evidence for a Shallowly Stratified Ocean Following the Triassic-Jurassic Boundary Mass Extinction. *Geochimica et Cosmochimica Acta* 231, 73–87. doi:10.1016/j.gca.2018.04.015

Mancinelli, A., Chiocchini, M., Chiocchini, R. A., and Romano, A. (2005). Biostratigraphy of Upper Triassic-Lower Jurassic Carbonate Platform Sediments of the central-southern Apennines (Italy). *Riv. Ital. di Paleontol. e Stratigr.* 111, 314. doi:10.13130/2039-4942/6314

Maréchal, C. N., Nicolas, E., Douchet, C., and Albarède, F. (2000). Abundance of Zinc Isotopes as a marine Biogeochemical Tracer. *Geochem. Geophys. Geosyst.* 1, 29. doi:10.1029/1999GC000029

Martini, R., Cirilli, S., Saurer, C., Abate, B., Ferruzza, G., and Lo Cicero, G. (2007). Depositional Environment and Biofacies Characterisation of the Triassic (Carnian to Rhaetian) Carbonate Succession of Punta Bassano (Marettimo Island, Sicily). *Facies* 53, 389–400. doi:10.1007/s10347-007-0115-3

Marzoli, A., Bertrand, H., Knight, K. B., Cirilli, S., Buratti, N., Vérati, C., et al. (2004). Synchrony of the Central Atlantic Magmatic Province and the Triassic-Jurassic Boundary Climatic and Biotic Crisis. *Geol* 32, 973–976. doi:10.1130/G20652.1

Marzoli, A., Renne, P. R., Piccirillo, E. M., Ernesto, M., Bellieni, G., and Min, A. D. (1999). Extensive 200-Million-Year-Old continental Flood Basalts of the Central Atlantic Magmatic Province. *Science* 284, 616–618. doi:10.1126/science.284.5414.616

McArthur, J. M., Howarth, R. J., and Bailey, T. R. (2001). Strontium Isotope Stratigraphy: LOWESS Version 3: Best Fit to the Marine Sr-Isotope Curve for 0-509 Ma and Accompanying Look-up Table for Deriving Numerical Age. *J. Geology.* 109, 155–170. doi:10.1086/319243

McElwain, J. C., Beerling, D. J., and Woodward, F. I. (1999). Fossil Plants and Global Warming at the Triassic-Jurassic Boundary. *Science* 285, 1386–1390. doi:10.1126/science.285.5432.1386

McRoberts, C. A., Krystyn, L., and Hautmann, M. (2012). Macrofaunal Response to the End-Triassic Mass Extinction in the West-Tethyan Kossen Basin, Austria. *Palaios* 27, 607–616. doi:10.2110/palo.2012.p12-043r

Nigro, F., and Renda, P. (2002). From Mesozoic Extension to Tertiary Collision: Deformation Patterns in the Units of the North-Western Sicilian Chain. *Bolletino Della Soc. Geol. Ital.* 121, 87–97.

Patacca, E., Scandone, P., Giunta, G., and Liguori, V. (1979). Mesozoic Paleo-Tectonic Evolution of the Ragusa Zone (southeastern Sicily). *Geol. Rom.* 18, 331–369.

Randazzo, V., Di Stefano, P., Todaro, S., and Cacciatore, M. S. (2020a). A Cretaceous Carbonate Escarpment from Western Sicily (Italy): Biostratigraphy and Tectono-Sedimentary Evolution. *Cretaceous Res.* 110, 104423. doi:10.1016/j.cretres.2020.104423

Randazzo, V., Le Goff, J., Di Stefano, P., Reijmer, J., Todaro, S., and Cacciatore, M. S. (2020b). Carbonate Slope Re-sedimentation in a Tectonically-active Setting (Western Sicily Cretaceous Escarpment, Italy). *Sedimentology* 67, 2360–2391. doi:10.1111/sed.12705

Raup, D. M., and Sepkoski, J. J., Jr (1982). Mass Extinctions in the marine Fossil Record. *Science* 215, 1501–1503. doi:10.1126/science.215.4539.1501

Romano, R., Masett, D., Carras, N., Barattolo, F., and Roghi, G. (2008). The Triassic/Jurassic Boundary in a Peritidal Carbonate Platform of the Pelagonian Domain: The Mount Messapion Section (Chalkida, Greece). *Riv. Ital. di Paleontol. e Stratigr.* 114, 431–452. doi:10.13130/2039-4942/5910

Ruhl, M., Bonis, N. R., Reichart, G.-J., Damsté, J. S. S., and Kürschner, W. M. (2011). Atmospheric Carbon Injection Linked to End-Triassic Mass Extinction. *Science* 333, 430–434. doi:10.1126/science.1204255

Ruhl, M., Kürschner, W. M., and Krystyn, L. (2009). Triassic-Jurassic Organic Carbon Isotope Stratigraphy of Key Sections in the Western Tethys Realm (Austria). *Earth Planet. Sci. Lett.* 281, 169–187. doi:10.1016/j.epsl.2009.02.020

Ruhl, M., and Kürschner, W. M. (2011). Multiple Phases of Carbon Cycle Disturbance from Large Igneous Province Formation at the Triassic-Jurassic Transition. *Geology* 39, 431–434. doi:10.1130/G31680.1

Schaller, M. F., Wright, J. D., and Kent, D. V. (2011). Atmospheric P Co 2 Perturbations Associated with the Central Atlantic Magmatic Province. *Science* 331, 1404–1409. doi:10.1126/science.1199011

Schobben, M., Van De Schootbrugge, B., and Wignall, P. B. (2019). Interpreting the Carbon Isotope Record of Mass Extinctions. *Elem. Int. Mag. Mineral. Geochemistry, Petrol.* 15, 331–337. doi:10.2138/gselements.15.5.331

Senowbari Daryan, B., Di Stefano, P., and Abate, B. (2015). Hypercalcified Sponges from the Upper Triassic (Norian-Rhaetian) Reefs of Sicily. *Quaderni Del. Museo Geologici G.G. Gemmellaro* 10, 1–300.

Sepkoski, J. J., Jr (1994). Extinction and the Fossil Record. *Geotimes* 39, 15–17.

Song, H., Kemp, D. B., Tian, L., Chu, D., Song, H., and Dai, X. (2021). Thresholds of Temperature Change for Mass Extinctions. *Nat. Commun.* 12, 4694. doi:10.1038/s41467-021-25019-2

Suarez, C. A., Edmonds, M., and Jones, A. P. (2019). Earth Catastrophes and Their Impact on the Carbon Cycle. *Elem. Int. Mag. Mineral. Geochemistry, Petrol.* 15, 301–306. doi:10.2138/gselements.15.5.301

Todaro, S., Agosta, F., Parrino, N., Cavalcante, F., Di Stefano, P., Giarrusso, R., et al. (2022). Fracture Stratigraphy and Oil First Migration in Triassic Shales, Favignana Island, Western Sicily, Italy. *Mar. Pet. Geology.* 135, 105400. doi:10.1016/j.marpetgeo.2021.105400

Todaro, S., Di Stefano, P., Zarcone, G., and Randazzo, V. (2017). Facies Stacking and Extinctions across the Triassic-Jurassic Boundary in a Peritidal Succession from Western Sicily. *Facies* 63, 20. doi:10.1007/s10347-017-0500-5

Todaro, S., Rigo, M., Randazzo, V., and Di Stefano, P. (2018). The End-Triassic Mass Extinction: A New Correlation between Extinction Events and δ13C Fluctuations from a Triassic-Jurassic Peritidal Succession in Western Sicily. *Sediment. Geology.* 368, 105–113. doi:10.1016/j.sedgeo.2018.03.008

Todaro, S., Sulli, A., Spatola, D., Micallef, A., Di Stefano, P., and Basilone, G. (2021). Depositional Mechanism of the Upper Pliocene-Pleistocene Shelf-Slope System of the Western Malta Plateau (Sicily Channel). *Sediment. Geology.* 417, 105882. doi:10.1016/j.sedgeo.2021.105882

Van De Schootbrugge, B., Payne, J. L., Tomasovych, A., Pross, J., Fiebig, J., Benbrahim, M., et al. (2008). Carbon Cycle Perturbation and Stabilization in the Wake of the Triassic-Jurassic Boundary Mass-Extinction Event. *Geochem. Geophys. Geosyst.* 9, a–n. doi:10.1029/2007GC001914

van de Schootbrugge, B., and Wignall, P. B. (2016). A Tale of Two Extinctions: Converging End-Permian and End-Triassic Scenarios. *Geol. Mag.* 153, 332–354. doi:10.1017/S0016756815000643

Végh-Neubrandt, E. (1982). *Triassische Megalodontaceae*: Entwicklung, Stratigraphie und Paläontologie. Budapest: Akadémiai kiadó, 1–526.

Veizer, J. (1989). Strontium Isotopes in Seawater through Time. *Annu. Rev. Earth Planet. Sci.* 17, 141–167. doi:10.1146/annurev.ea.17.050189.001041

Wignall, P. B., and Atkinson, J. W. (2020). A Two-phase End-Triassic Mass Extinction. *Earth-Science Rev.* 208, 103282. doi:10.1016/j.earscirev.2020.103282

Wignall, P. B. (2001). Large Igneous Provinces and Mass Extinctions. *Earth-Science Rev.* 53, 1–33. doi:10.1016/S0012-8252(00)00037-4

Wignall, P. B., Zonneveld, J.-P., Newton, R. J., Amor, K., Sephton, M. A., and Hartley, S. (2007). The End Triassic Mass Extinction Record of Williston Lake, British Columbia. *Palaeogeogr. Palaeoclimatol. Palaeoecol.* 253, 385–406. doi:10.1016/j.palaeo.2007.06.020

Yancey, T. E., and Stanley, Jr, G. D. (1999). Giant Alatoform Bivalves in the Upper Triassic of Western North America. *Palaeontology* 42, 1–23. doi:10.1111/1475-4983.00060

Zaffani, M., Jadoul, F., and Rigo, M. (2018). A New Rhaetian δ13Corg Record: Carbon Cycle Disturbances, Volcanism, End-Triassic Mass Extinction (ETE). *Earth-Science Rev.* 178, 92–104. doi:10.1016/j.earscirev.2018.01.004

Zarcone, G., and Di Stefano, P. (2010). La Piattaforma Carbonatica Panormide:un caso anomalo nell'evoluzione dei bacini della Tetide giurassica. *Ital. J. Geosci.* 129, 188–194. doi:10.3301/IJG.2010.01

Zarcone, G., Petti, F. M., Cillari, A., Di Stefano, P., Guzzetta, D., and Nicosia, U. (2010). A Possible Bridge between Adria and Africa: New Palaeobiogeographic and Stratigraphic Constraints on the Mesozoic Palaeogeography of the Central Mediterranean Area. *Earth-Science Rev.* 103, 154–162. doi:10.1016/j.earscirev.2010.09.005

Conflict of Interest: The authors declare that the research was conducted in the absence of any commercial or financial relationships that could be construed as a potential conflict of interest.

Publisher's Note: All claims expressed in this article are solely those of the authors and do not necessarily represent those of their affiliated organizations, or those of the publisher, the editors, and the reviewers. Any product that may be evaluated in this article, or claim that may be made by its manufacturer, is not guaranteed or endorsed by the publisher.